[2021 Summer/Fall] KAIST URP Program

Individual Research Project Final Report

Creative Project

아연-망간 전해 전지 시스템 개발 및 주요 운용 조건 파악에 관한 연구

Developing Electrolytic Zn-Mn Battery System and Identifying Key Operation Conditions

생명화학공학과 김태우 (20190192)

For Submission

Research Subject (Korean): 아연-망간 전해 전지 시스템 개발 및 주요 운용 조건 파악에 관한 연구

Research Subject (English): Developing Electrolytic Zn-Mn Battery System and Identifying Key Operation Conditions

Research Period: June 28, 2021 ~ December 17, 2021

Advisory Professor: 김 희 탁 **(Signature)**

Teaching Assistant: 신 경 재 **(Signature)**

As a participant(s) of the KAIST URP program, I (We) have completed the above research and hereby submit the final report on the research.

December 24, 2021

Researcher 김 태 우 **(Signature)**

Contents

Abstract

The fire hazard of lithium-ion batteries has motivated the development of more efficient and safer battery technology for energy storage systems (ESSs). An electrolytic zinc manganese oxide battery system (EZMB) can offer a possibility of a cost-effective and non-flammable ESS. However, toward the development of a practical battery, many critical issues should be addressed. In this research, we developed an EZMB system single cell to identify key operation conditions with cell-level perspective. The acidity variation resulted from HER at the negative electrode resulted in irreversible MnO_2 deposition/dissolution reaction with increasing the proportion of non-faradaic reaction at the electrode. With the electrolyte acidity management by implementing the electrolyte reservoir, the EZMB system showed greatly enhanced cycle performance of more than 500 cycles at high areal capacity of 1.90 mAh/cm^2 under current density of 2 mA/cm^2 showing stable performance with coulombic efficiency of 95.1% and energy efficiency of 70.5% in average.

1. Research Background

Renewable energies have the disadvantage of intermittent energy generation depending on the environmental condition. To overcome this issue, energy storage system (ESS) plays an important role of storing and releasing the energy on demand by converting the electrical energy into chemical energy [1]. However, conventional ESSs are mostly based on the lithium-ion batteries, which have inherent flammability and resulting safety issue [2, 3].

Non-flammable aqueous batteries can be a promising solution for the safety concern of conventional ESSs because of the non-flammability of the electrolyte [4, 5]. Various aqueous batteries have been reported, such as vanadium redox flow batteries [6, 7], zinc-bromine redox flow batteries [8, 9]. However, as these systems store energy in the form of electrolyte, redox active material cross over result in performance degradation with the self-discharge reaction. Although, in order to mitigate the self-discharge reaction, ion-exchange membrane or highly porous membrane can be introduced, expensive cost of those membranes, such as Nafion, increases the system cost [10, 11]. Recently, Prof. S. Z. Qiao group in the University of Adelaide reported innovative strategy of utilizing zinc and manganese oxide as redox active materials called electrolytic zinc manganese oxide battery (EZMB). As the redox active materials are stored on the surface of the electrodes in solid phase, EZMBs do not suffer from the cross-over issue. In this perspective, the EZMB seems promising candidate for cost effective and safe ESSs.

2. Research Purpose

Previously reported EZMB configuration shows limited areal capacity. This is resulted from the limited amount of electrolyte accommodation of the design. As the redox active material of EZMB is stored in the electrolyte, the theoretical capacity of EZMB can be easily modulated with the amount of electrolyte volume. This strategy seems promising because of the abundant zinc and manganese oxide. However, as the standard redox potential of zinc metal deposition/dissolution lies below that of HER, the system will continuously suffer from the HER reaction, which will affect activity of manganese oxide deposition. This acidity variation can affect more severely with large electrolyte accommodation, with excess amount H_2O to be decomposed. Thus, in this research, we developed a large capacity flowless EZMB and identified the influence of acidity variation on the system performance.

3. Experimental Methods

3.1 Materials

All of the chemicals were purchased from Sigma Aldrich at analytical grade and used without further purification. The graphite felt was purchased from SGL(GFD4.6) and used as electrodes. The carbon felt was thermally oxidized in tube furnace. The temperature was gently elevated at the rate of 5 ℃/min to 520 ℃ and held at the temperature for 7 h 20 min under the ambient air condition. After the thermal oxidization, the furnace was cooled to the room temperature. The zinc metal foil was purchased from Alfa Aesar and used without further purification.

3.2 EZMB single cell construction

The proposed Zn-MnO_2 aqueous flowless battery consists of end plates, current collectors, bipolar plates, carbon felt (positive electrode), electrolyte, zinc metal plate (negative electrode), and chamber. At the chamber, vent is introduced where electrolyte or gas can freely flow. For the electrolyte, 1 M $ZnSO_4$, 1 M $MnSO_4$ and 0.1 M H_2SO_4 were dissolved in DI water. Detailed explanation of the structure is shown in Fig. 1.

3.3 Electrochemical analysis

The electrochemical performance analysis was measured with WSBC3000(Won-A Tech) for the designed EZMB single cell. For the cycle test, the cell is charged at the constant voltage of 2.2 V (vs. Zn/Zn^{2+}) with capacity cut of 2 mAh/cm^2 and discharged at constant current density of 2 mA/cm^2. The cut-off voltage for the discharge step was 0.8 V (vs. Zn/Zn^{2+}).

In order to understand the electrochemical reaction transition, cyclic voltammetry and electrochemical impedance spectroscopy test was conducted with specific cycle period. The CV and EIS was measured using VSP(Biologics). For CV, cells were scanned from 0.8 V to 2.2 V (vs. Zn/Zn^{2+}) using zinc metal tab as a reference electrode. Scan rate was 0.1 mV/s. The scan was repeated 3 times. For EIS test, cells were scanned from the frequency 10000.0 Hz to 0.01 Hz. The sinus amplitude of the voltage was 10.0 mV.

3.4 Characterization

SEM analysis of gradual growth of the MnO_2 on the surface of the carbon felt electrode was performed using Field-Emission Scanning Electron Microscope (FE-SEM, Sirion by FEI) with 1-kV accelerating voltage and 5.0mm working distance(Z-height). To prepare samples for the analysis, all samples were gently rinsed with DI in order to remove surface contaminant and residual salts.

4. Results

4.1 Designing a flowless EZMB single cell

The unit cell is composed of end plates, current collectors, bipolar plates, carbon felt (cathode), electrolyte, zinc metal plate (anode), and the chamber with a vent. The end plates are used to cover the entire cell. Current collectors are made of copper, and collects the current flow. Bipolar plates enable the system to be stacked up, which is advantageous for large scale ESS [12]. Chamber contains electrolyte and the electrochemical reaction is held. Chamber has a little circular vent, which is designed for releasing gas that might be generated from electrolyte decomposition inside the cell. Below Fig. 2. is the photo of assembled cell based on the Fig. 1.

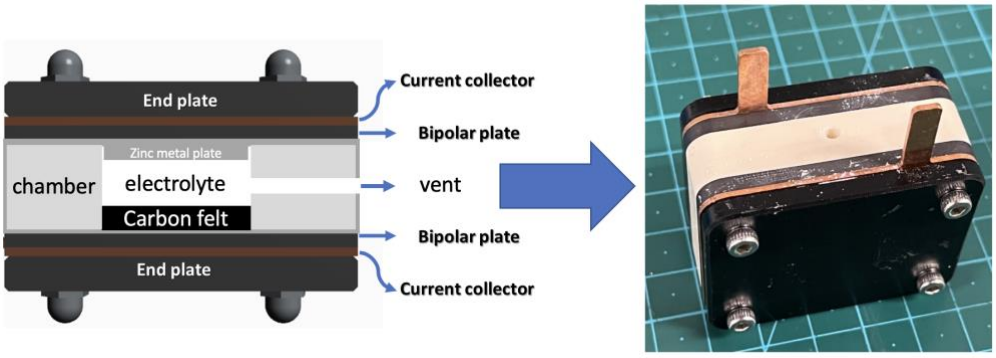

Figure 1. Assembled cell based on the Fig. 1 scheme

The unit cell capacity can be modulated with the amount of electrolyte volume as the redox active materials are stored in the form of electrolyte. With the electrode distance expansion, large amount of electrolyte can be accommodated and the capacity can be increased.

4.2 Morphology variation of the positive electrode during charging process

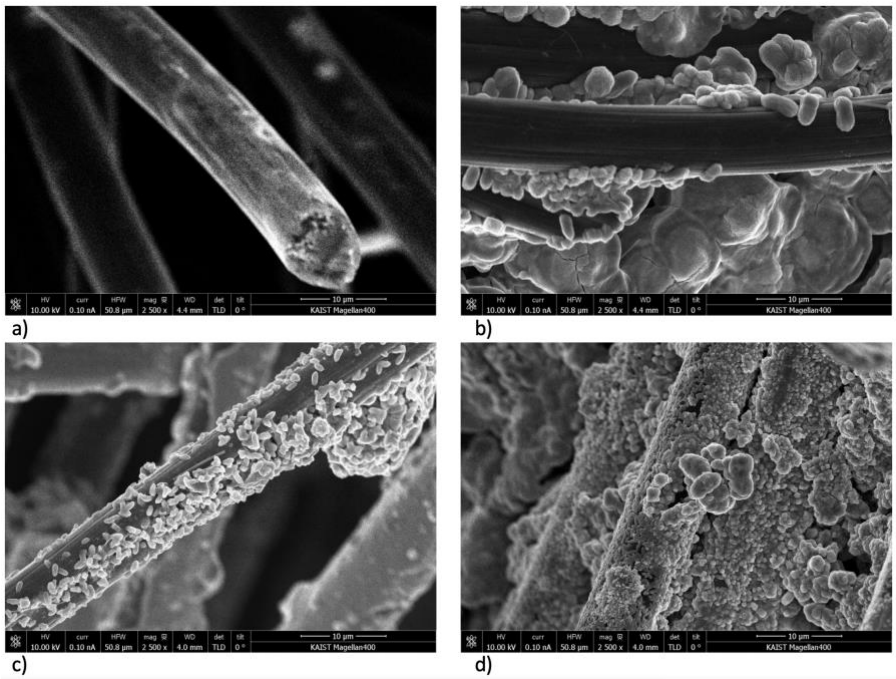

Figure 2. a) Pristine carbon cloth cathode. b) Cathode surface at 2 mAh/cm^2. c) Cathode surface at 4 mAh/cm^2. d) Cathode surface at 8 mAh/cm^2.

Fig. 2 shows the SEM image of the positive electrode surface of the pristine carbon cloth and when the cell is charged to 2, 4, 8 mAh/cm^2. The SEM image reveals well-deposited MnO_2 nanoparticles. MnO_2 nano-particles are nucleated and deposited on the surface of the carbon fiber during charging process. As the depth of the charge increases, the MnO_2 nanoparticles are agglomerated and cover the entire surface.

4.3 System operation condition identification

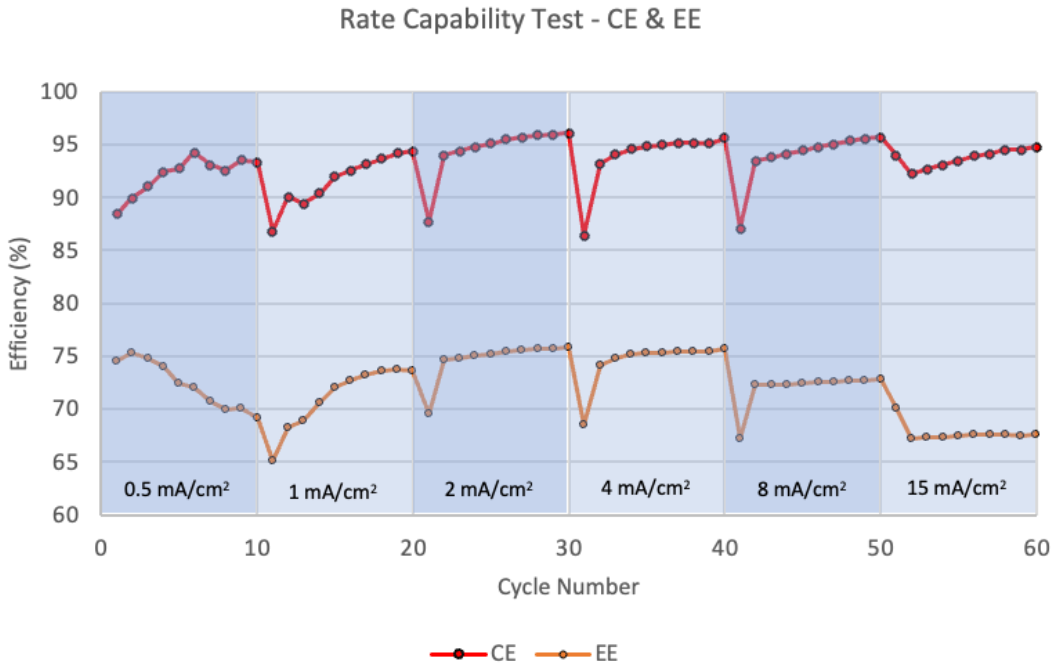

Figure 3. Coulombic and energy efficiency during the rate capability test of EZMB single cell

As given in Fig. 3, in order to identify proper operation current density, rate capability test was conducted, comparing efficiencies at various current densities. The coulombic efficiency (CE) and energy efficiency (EE) of the cell was the highest in 2 mA/cm^2 region (21st ~ 30th cycle), which is 94.5% for CE and 74.8% for EE in average, which seems to be related with the irreversible redox reaction of MnO2 deposition [13]. Therefore, 2 mA/cm^2 was picked for the discharging current density condition.

4.4 Discharge capacity degradation

When the cell with closed vent repeats charging and discharging, the electrolyte was severely leaked as shown in the Fig. 4. The leakage of the electrolyte is assumed to be related with HER at the negative electrode.

Figure 4. Severe electrolyte leakage of EZMB single cell

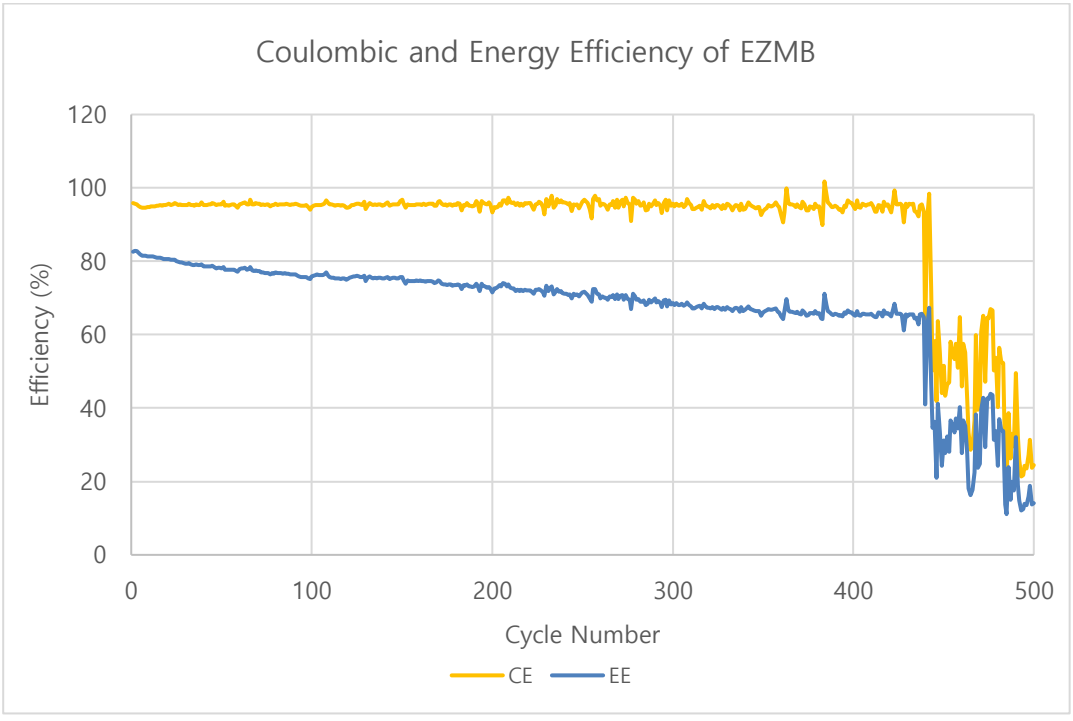

Figure 5. Long-term CE and EE of EZMB single cell

Also, the decrease of the discharge capacity, was observed as shown in the Fig. 4. To understand the reason of degradation, discharging voltage profiles at the early and late stage of the cell operation were examined.

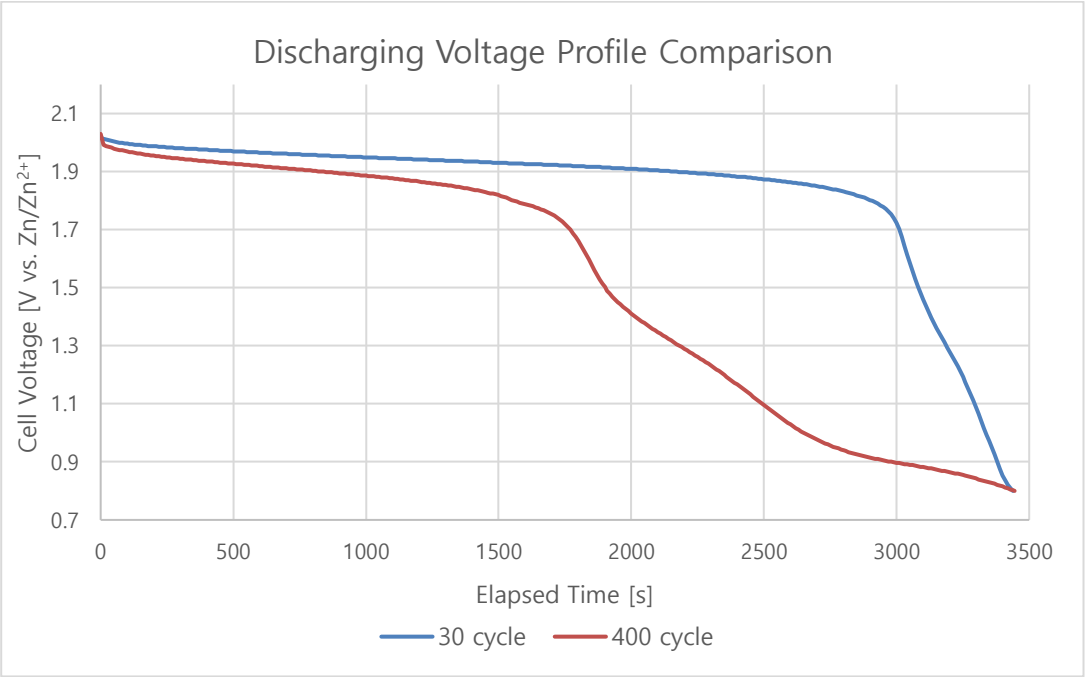

Figure 6. Discharging voltage profile comparison between after 30th cycle and 400th cycle

At the later cycle, the voltage decreased more quickly. Chao DL et al. [13] showed voltage profiles at various proton concentration of electrolyte in EZMB. We found that our later cycle profile looks similar to the case of higher pH of electrolyte. This could be possible because the pH of the electrolyte would increase as the HER consumes the H^+.

Also, inflection points are observed near 1.5 V and 0.9 V at the later cycle. This seems to be related with Zn^{2+} cation intercalation into MnO_2 [14, 15]. For the accurate explanation, cyclic voltammetry (CV) and electrochemical impedance spectroscopy (EIS) test were done at the specific cycle period (50th, 150th, 250th).

4.5 Electrochemical analysis

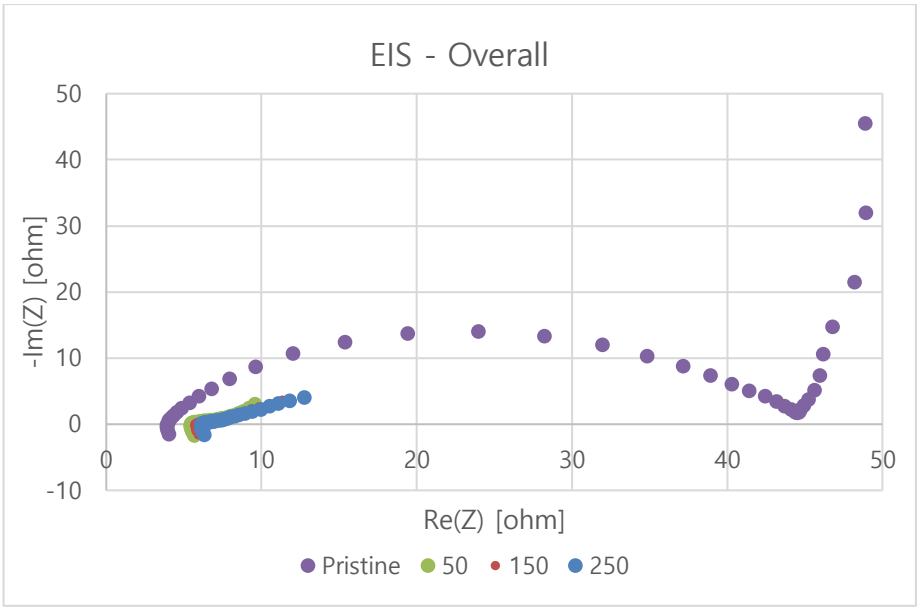

a)

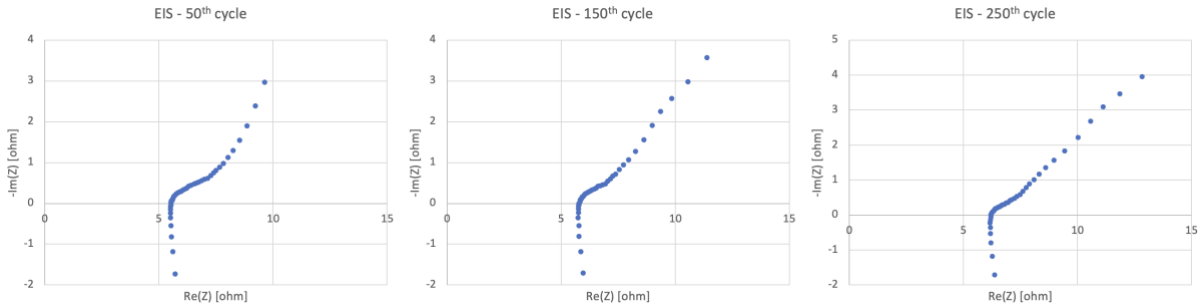

b) c) d)

Figure 7. a) Overall EIS test result. Result for b) after 50 cycles, c) after 150 cycles, d) after 250 cycles are magnified below.

In order to identify the reaction mechanism transition at the positive electrode, the electrochemical EZMB single cell was electrochemically analyzed with EIS. As given in Fig. 7, the Nyquist plot of pristine cell shows both ohmic resistance and charge transfer resistance. With the cycle number increment, the ohmic resistance showed increase with charge transfer resistance disappearance. The increased ohmic resistance is related with the accumulation of insulating MnO_2 nano-particles. As the insulator cover-up the active area, decreased active area resulted in larger ohmic resistance. Furthermore, the disappearance of charge transfer resistance was also observed after 50^{th} cycles. It indicates that the reaction mechanism transition from faradaic to non-faradaic reaction mechanism.

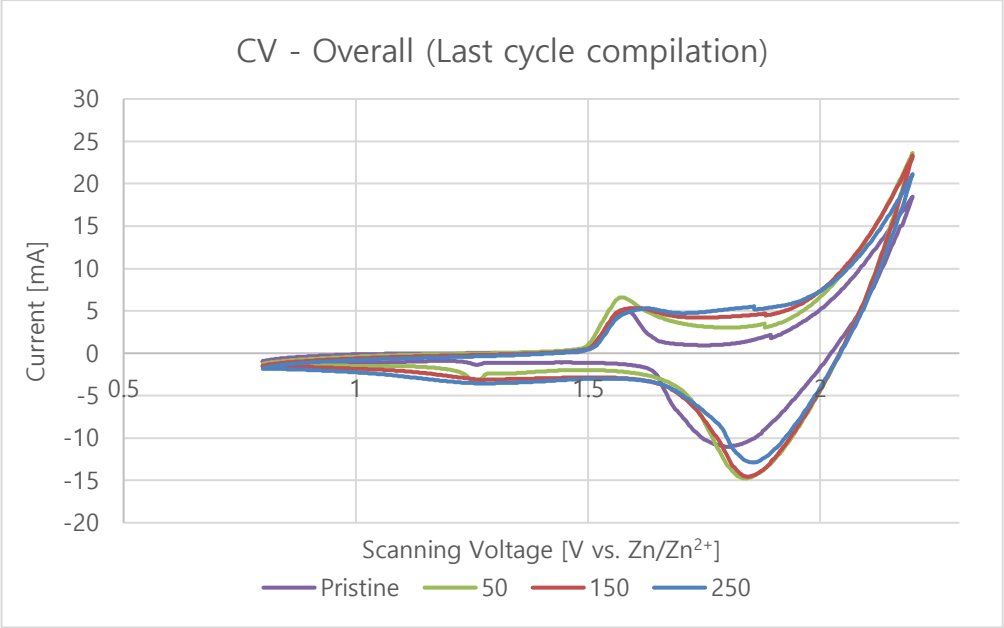

Figure 8. Overall CV result. Only last cycles of CV test are compiled for comparison.

Similar trend can be observed with CV profile as given in Fig. 8. For the pristine cells, well developed anodic and oxidative peaks are observed. However, as the cycle prolongs, the cathodic peak showed merging into planar current region without showing peak. However, in the case of anodic peak, well developed peak is observed. This difference between anodic/cathodic peak seems to be related with the fact that during the anodic scan, Mn^{2+} cation approaches to the electrode surface and oxidized. As the active area is covered insulating MnO_2, the Mn^{2+} cation is hindered from oxidation. Thus, mere capacitive current is observed. On the contrary, in cathodic scan, the pre-deposited MnO_2 can easily be reduced as the layer is deposited on conducting carbon felt electrode. From the electrochemical analysis, it can be concluded that the continuous proton consumption resulted in pH variation during system operation. The increased pH accelerates irreversible MnO_2 deposition/dissolution at the positive electrode and leads the reaction mechanism to change from faradaic to non-faradaic reaction. Thus, for the stable operation of flowless EZMB, the electrolyte pH management seems to be important to retard reaction mechanism transition from faradaic to non-faradaic reaction.

4.6 Cycle performance with pH management

In order to manage the electrolyte pH during operation, an electrolyte reservoir was connected to the EZMB single cell as given in Fig. 9 and compared to the case without the reservoir.

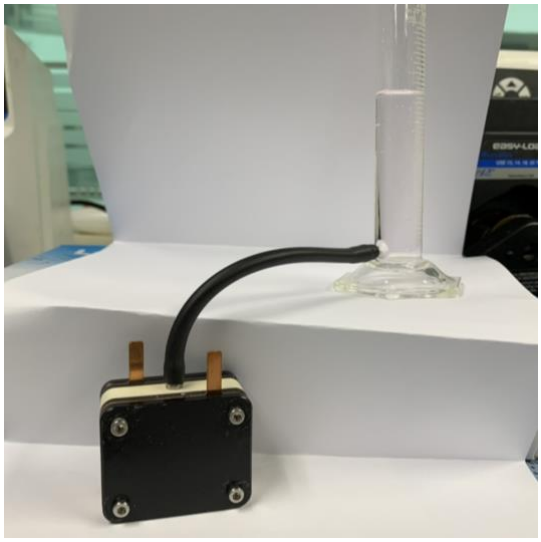

Figure 9. Experimental setup of the EZMB single cell with reservoir

Fig. 10 shows the cycle data of the EZMB cell with/without the reservoir. The cell without the reservoir showed significant decrease in efficiency at around 450th cycle. However, in case of the cell with the reservoir, it was maintained until 500th cycle without any significant drop in the efficiency. This graph also suggests that the cell with the reservoir could operate well over 500th cycle. This is because the acidity of the electrolyte was preserved well by the electrolyte reservoir, resulting the cell reaction mechanism to stay faradaic. The average coulombic efficiency and energy efficiency of the cell with reservoir during the 500 cycles were 95.1% and 70.5%, respectively.

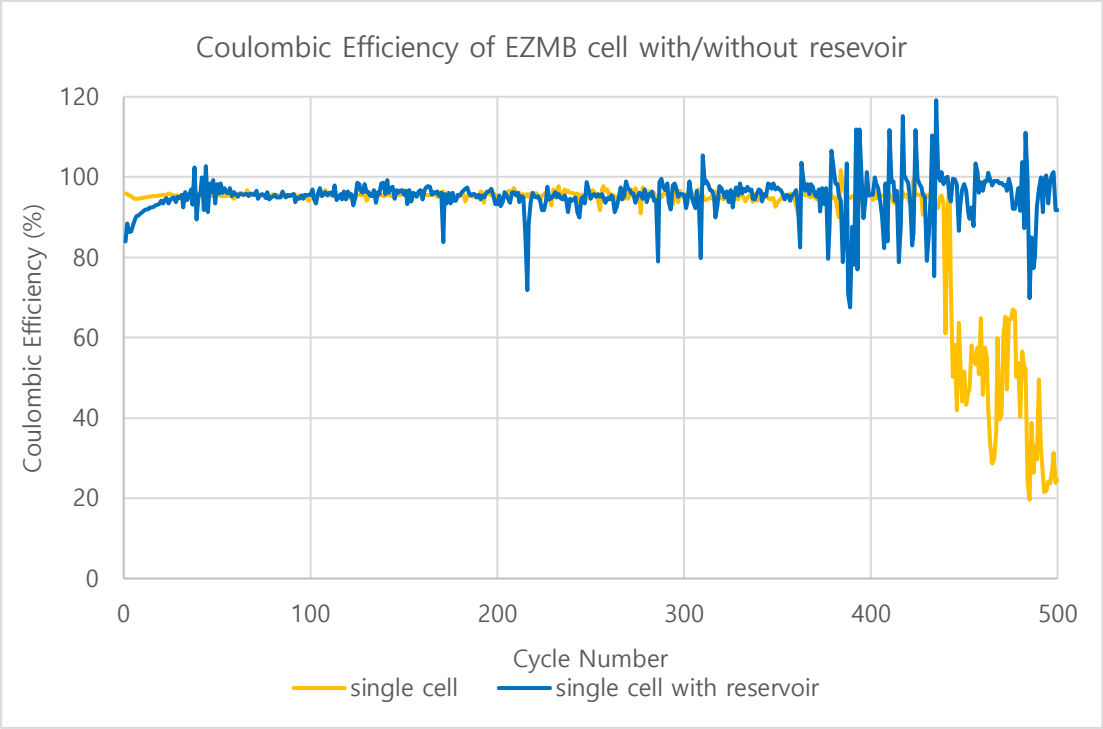

a)

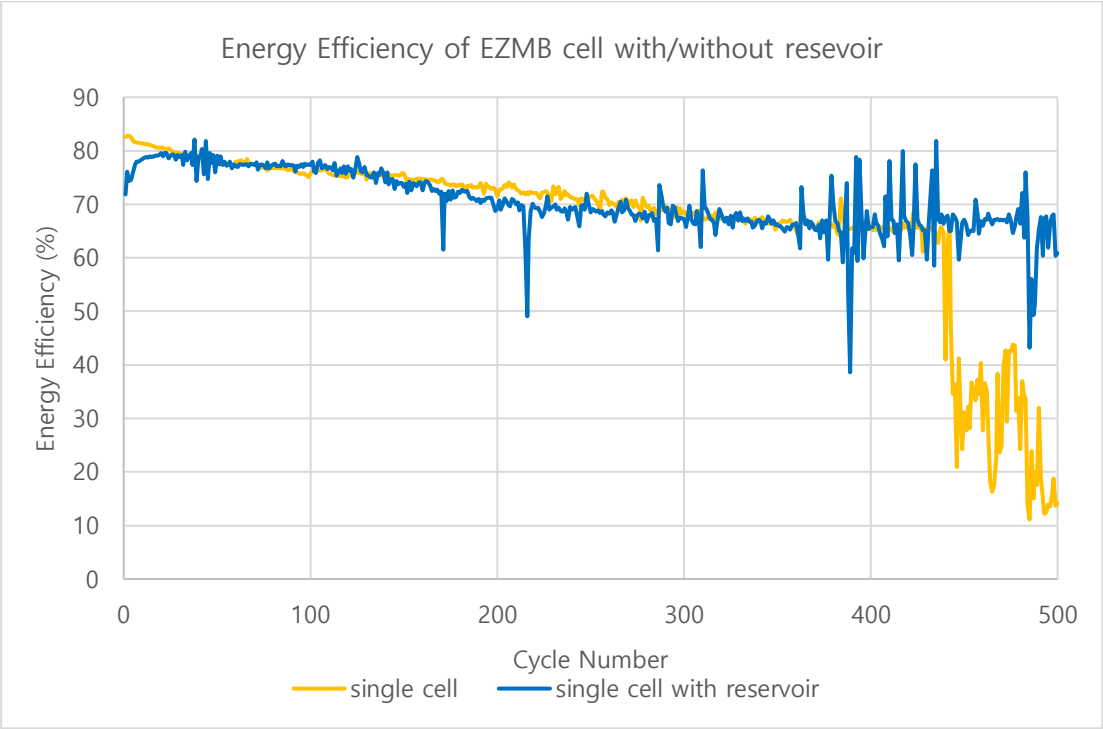

b)

Figure 10. a) Coulombic efficiency and b) energy efficiency of the EZMB cell with/without reservoir

5. Conclusion

An EZMB single cell was developed and well operated. During the operation, the cell showed severe electrolyte leakage and decrease in discharge capacity as the charging/discharging cycle proceeds. By analyzing the CV and EIS test at the specific cycle period, it was identified that change in pH of electrolyte was the major effect of the decreasing capacity. As the cell cycle increases, the pH of the electrolyte increases because of the proton consumption by HER. This made the MnO_2 deposition/dissolution reaction irreversible, so the overall cell reaction became non-faradaic. Therefore, maintaining the pH of the electrolyte low has an important role for long-lasting and high-performance EZMB.

6. Future Research Plan & Proposal

Setting up the experimental operation condition took much longer than we expected, because we tested various cell configuration and had trial-and-error to find the optimum system. Also, each experimental step like long-term cycle test and CV test took very long, so we couldn't reach the goal to develop the high-performance cathode material due to the time limit. If it comes to the point, we want to resume the research based on our result.

We conjectured that pH of the electrolyte could also affect the cell degradation mechanism. So, we wanted to measure the pH of the electrolyte with various cycles. However, since the volume of the electrolyte was so small, measuring pH was not easy. We also want to do that in the future research.

Developing an electrode that induces reversible deposition/dissolution of MnO_2 can dramatically increase the long-term stability of the cell. Also, if possible, we want to measure the pH of electrolyte during the cycle test to correlate the pH and cell efficiency more precisely.

7. Reference Literature

[1] Yao X, Yi BW, Yu Y *et al.* Economic analysis of grid integration of variable solar and wind power with conventional power system. Appl Energ 2020; 264.
[2] Larsson F, Andersson P, Mellander BE. Lithium-Ion Battery Aspects on Fires in Electrified Vehicles on the Basis of Experimental Abuse Tests. Batteries-Basel 2016; 2.
[3] Larsson F, Andersson P, Blomqvist P, Mellander BE. Toxic fluoride gas emissions from lithium-ion battery fires. Scientific Reports 2017; 7.
[4] Fang G, Zhou J, Pan A, Liang S. Recent advances in aqueous zinc-ion batteries. ACS Energy Letters 2018; 3:2480-2501.
[5] Zhang L, Rodriguez-Perez IA, Jiang H *et al.* ZnCl2 "Water-in-Salt" Electrolyte Transforms the Performance of Vanadium Oxide as a Zn Battery Cathode. Adv Funct Mater 2019; 29.
[6] Heo J, Hang JY, Kim S *et al.* Catalytic production of impurity-free V3.5+ electrolyte for vanadium redox flow batteries. Nature Communications 2019; 10.
[7] He HY, Tian S, Tarroja B *et al.* Flow battery production: Materials selection and environmental impact. J Clean Prod 2020; 269.
[8] Kim H-T, Lee J-H, Kim DS, Yang JH. Redox Flow – Zn–Br. In: Encyclopedia of Electrochemistry. pp. 1-38.
[9] Rajarathnam GP, Vassallo AM. The Zinc/Bromine Flow Battery : Materials Challenges and Practical Solutions for Technology Advancement. In: SpringerBriefs in Energy,. 1st. Singapore: Springer Singapore : Imprint: Springer,; 2016. pp. 1 online resource (XXI, 97 pages 31 illustrations, 26 illustrations in color.
[10] Kim S, Choi J, Choi C *et al.* Pore-Size-Tuned Graphene Oxide Frameworks as Ion-Selective and Protective Layers on Hydrocarbon Membranes for Vanadium Redox-Flow Batteries. Nano Lett 2018; 18:3962-3968.
[11] Lee JH, Byun Y, Jeong GH *et al.* High-Energy Efficiency Membraneless Flowless Zn-Br Battery: Utilizing the Electrochemical-Chemical Growth of Polybromides. Adv Mater 2019; 31.
[12] Evanko B, Yoo SJ, Lipton J *et al.* Stackable bipolar pouch cells with corrosion-resistant current collectors enable high-power aqueous electrochemical energy storage. Energ Environ Sci 2018; 11:2865-2875.
[13] Chao DL, Zhou WH, Ye C *et al.* An Electrolytic Zn-MnO2 Battery for High-Voltage and Scalable Energy Storage. Angew Chem Int Edit 2019; 58:7823-7828.
[14] Zhong C, Liu B, Ding J *et al.* Decoupling electrolytes towards stable and high-energy rechargeable aqueous zinc-manganese dioxide batteries. Nat Energy 2020; 5:440-449.
[15] Liao Y, Chen H-C, Yang C *et al.* Unveiling performance evolution mechanisms of MnO2 polymorphs for durable aqueous zinc-ion batteries. Energy Storage Materials 2022; 44:508-516.